Wide Band Modeling of Power Transformers

Bjørn Gustavsen, *Senior Member, IEEE*

***Abstract*—This paper describes the measurement setup and modeling technique used for obtaining a linear wide band frequency-dependent black box model of a two-winding power transformer, for the purpose of calculation of electromagnetic transients in power systems. The measurement setup is based on a network analyzer, shielded cables, and a connection board. The setup is demonstrated to give a consistent data set where the effect of the measurement cables can be eliminated. The accuracy of the data set is increased by using a combination of current measurements and voltage transfer measurements. A rational approximation of the admittance matrix is calculated in the frequency domain in the range of 50 Hz to 1 MHz and subjected to passivity enforcement, giving a stable model which can be included in electromagnetic transients program (EMTP)-type simulation programs. The accuracy is validated both in the frequency domain and in the time domain.**

***Index Terms*—Electromagnetic transients, electromagnetic transients program, frequency dependence, measurement, power transformer, simulation, system identification.**

I. Introduction

THE high-frequency behavior of power transformers is characterized by several resonance points due to inductive and capacitive effects from the windings, tank, and core. This behavior should be included in any overvoltage study where the high-frequency characteristics of the transformer is of significance (e.g., transferred overvoltages and resonant overvoltages). The high-frequency behavior can be modeled by calculating a lumped electrical network based on geometry and material properties [1]–[4], but requires very detailed information about the transformer. A different approach is to calculate a black box model based on measured quantities at the transformer terminals [5]–[8]. Although a relatively large number of papers have been published on these two methods, few, if any, have demonstrated models which can reliably reproduce measured waveforms. Also, previous works have focused on frequencies from a few kilohertz and above, while it is desirable that the model be accurate also at power frequency in order to get the correct initial values in overvoltage simulations.

This paper describes in detail the instrumentation and measurement procedure used for obtaining the admittance matrix of a two-winding distribution transformer in the frequency range 50 Hz to 1 MHz. A procedure is shown for validation of the measured admittance matrix and for assessing the sensitivity due to measurement errors. A transformer model compatible with electromagnetic transients program (EMTP)-type programs is calculated by subjecting the admittance matrix to rational function approximation. The accuracy of the resulting model is validated by comparing measured and simulated waveforms in the time domain.

Manuscript received November 3, 2002. This work was supported by the European Commission's Directorate-General for Research through a Fifth Framework Programme Non Nuclear Energy Marie Curie Fellowship.

The author is with SINTEF Energy Research, Trondheim N-7465, Norway (e-mail: bjorn.gustavsen@energy.sintef.no).

Digital Object Identifier 10.1109/TPWRD.2003.820197

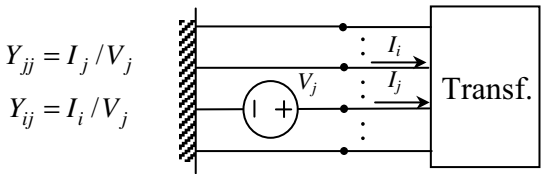

Fig. 1. Measuring elements of jth column of Y.

II. Measurements

A transformer terminal model can be formulated in the frequency domain in terms of its admittance matrix Y which defines the relation between terminal voltages V and terminal currents I

$$I(s) = Y(s)V(s). \tag{1}$$

For a transformer with n terminals, Y is a symmetric matrix of size n by n while I and V are vectors of length n.

It follows from (1) that applying 1-p.u. voltage to terminal j and zero voltage to the remaining terminals will produce the jth column of Y where element Y_{ij} is the current flowing from ground into terminal i. This permits the direct measurement of all elements of Y using a measurement procedure as outlined in Fig. 1.

The measurement errors may become magnified when using the obtained Y in a situation with a different terminal condition (e.g., when some terminals are open). It is therefore necessary to validate the model for different terminal conditions.

Consider the situation that the transformer terminals are divided into two groups, denoted by A and B, respectively. Appropriate numbering of the terminals permits Y to be partitioned

$$\begin{bmatrix} I_A \\ I_B \end{bmatrix} = \begin{bmatrix} Y_A & Y_B \\ Y_C & Y_D \end{bmatrix} \cdot \begin{bmatrix} V_A \\ V_B \end{bmatrix}. \tag{2}$$

If the terminals of set A are open-circuited ($I_{\mathrm{A}} = 0$), we get a voltage ratio

$$V_{AB} = -Y_A^{-1} Y_B. \tag{3}$$

Some transformer overvoltage studies involve the situation that all terminals of one winding are open circuited. For a two-winding transformer, we get from (3)

$$V_{HL} = -Y_{HH}^{-1} Y_{HL} \tag{4}$$

$$V_{LH} = -Y_{LL}^{-1} Y_{LH} \tag{5}$$

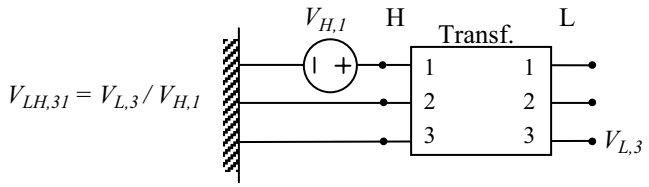

Fig. 2. Measuring element (3, 1) of V_{LH}.

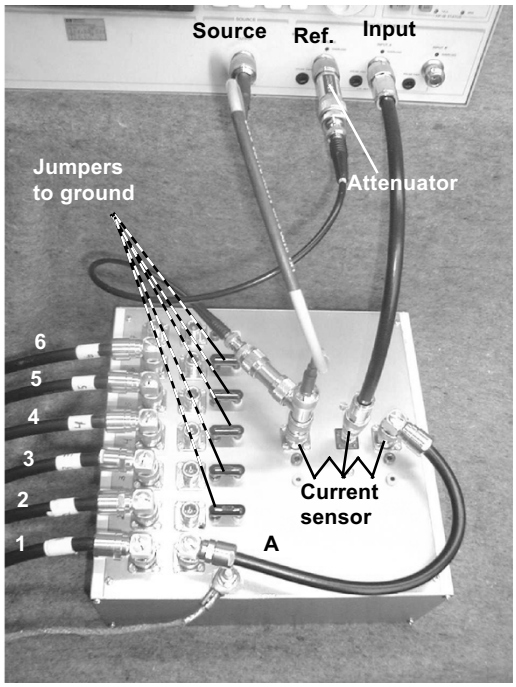

Fig. 3. Measuring Y_{11}.

where H and L denote the high-voltage and low-voltage windings. V_{HL} and V_{LH} are matrices of size 3 by 3.

A useful test is to compare the calculated V_{HL} and V_{LH} with a direct measurement of these quantities. The measurement procedure is illustrated in Fig. 2.

III. Measurement Setup

A. Instrumentation

A measurement setup has been designed for the purpose of measuring the admittance matrix Y as well as voltage ratios (e.g., V_{HL} and V_{LH}). The setup consists of a network analyzer, a connection board with a built-in current sensor (Fig. 3), and shielded cables which connect the transformer terminals with the connection board. The cable shields are grounded at both ends; at the transformer and at the connection board. All reconnections needed for measuring different matrix elements are done at the connection board using jumper connections, thus giving reproducible results. The cables between the network analyzer and the connection board are made as short as possible. The built-in calibration feature of the network analyzer is used for taking into account the frequency dependency of the current sensor, voltage probes, and the attenuator.

Fig. 3 shows the connection board as configured for the measurement of a diagonal element (Y_{11}). Fig. 4 shows the configuration used for measuring an off-diagonal element (Y_{13}). The following components were used:

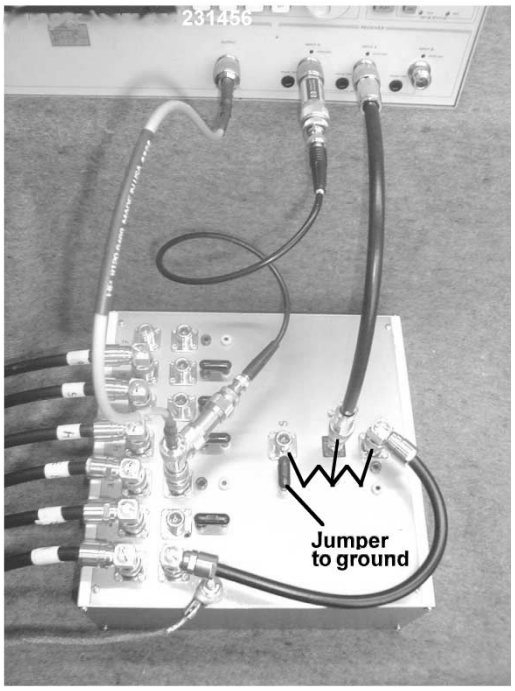

Fig. 4. Measuring Y_{13}.

1) network analyzer: HP3577A;
2) attenuator: HP8491A, 30 dB (a special attenuator with low-pass characteristic was used when connecting the source to the low-voltage winding);
3) current sensor: Pearson model 2100, 1 V/1 A.

All measurements were done using the following settings of the network analyzer: logarithmically distributed samples between 50 Hz and 2 MHz, 100-s sweep time, 10-Hz resolution bandwidth. After each sweep, the measured results were downloaded to a PC for further processing.

B. Correction for Measurement Cables

The dominant effect of the measurement cables is their capacitance to ground because the high impedance of the transformer prevents any significant voltage drop to develop along the cables. It follows that each cable i results in that the corresponding diagonal element Y_{ii} is modified by an added contribution sC_i with C_i being the cable capacitance. Thus, the major effect of the cables can be removed by correcting the measured Y using the expression

$$Y' = Y - sC \tag{6}$$

where C is a diagonal matrix with entries being the capacitance of the respective cables. The short stub cable "A" in Fig. 3 is taken into account by adding its capacitance to all diagonal elements of C.

IV. Accuracy Considerations

It follows from (3) that an open-circuit condition is equivalent to solving an equation $Ax = b$ with A and b being sub-

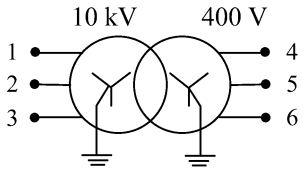

Fig. 5. Reconnected distribution transformer.

matrices of Y. It is well established in numerical linear algebra that when A and/or b contain errors, the error of the calculated x increases as the condition number κ_A of A increases. (The condition number is the ratio between the largest and smallest singular value of A.) Because the accuracy of the measured Y is inherently low (e.g., two or three digits precision), even a modest condition number can yield inaccurate results.

It is reasonable to assume that all elements in A and b can be measured with a common relative accuracy (e.g., 1%). If considering only the effects of errors in b it can be stated [9]: "The relative error in the solution x is smaller than or equal to the condition number multiplied with the relative error in data y." Thus, with a 1% relative error in y, a condition number exceeding 100 could cause a result x with an error as high as 100%. If considering a given (accurate) b and an A with a given *absolute* error, it can be stated [10]: "If solving an equation $Ax = b$ where A has condition number κ_A, one must expect to loose $\log_{10}(\kappa_A)$ digits in the process." The significance of a high condition number will be demonstrated in subsequent sections.

V. Frequency Domain Results

A. Measurement Object

As an example, a 30-kVA 10-kV/400-V distribution transformer ($e_k = 3.81\%$) with a Y-connected HV-winding and Z-connected LV-winding is considered. The transformer was opened and the winding terminals were brought to an external connection board, thus permitting the HV winding to be connected into Y or D, and the LV-winding to be connected into Y, D, or Z. In this paper, the situation is considered when both windings are connected as a grounded Y, see Fig. 5.

B. Admittance Matrix and Voltage Ratios

Fig. 6 shows the magnitude of the 36 measured elements of Y obtained with measurement cables of 5-m length. It is seen that the elements are strongly frequency dependent and that some elements are much smaller than others. The large difference in element sizes is mainly a result of the high voltage ratio of the transformer (25:1).

Fig. 7 compares the measured elements of V_{LH} with the corresponding elements calculated by (5). It is seen that the voltage transfer from high voltage to low voltage is at 200 kHz, about ten times higher than the voltage transfer at 50 Hz. The calculated ratio is seen to closely match the measured ratio.

A similar observation is made for the elements of V_{HL} when comparing measured and calculated quantities, see Fig. 8. Two distinct peaks of the transferred voltage can be observed around 15 kHz.

We next look at a situation with open terminals at both the HV and LV side, see Fig. 9. Fig. 10 compares the measured and calculated elements for the voltage ratio as calculated by (3). It is seen that a large deviation results at frequencies below 10 kHz.

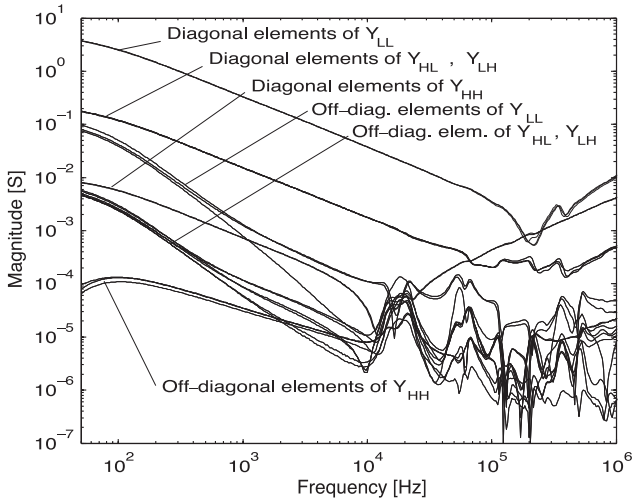

Fig. 6. Measured elements of Y.

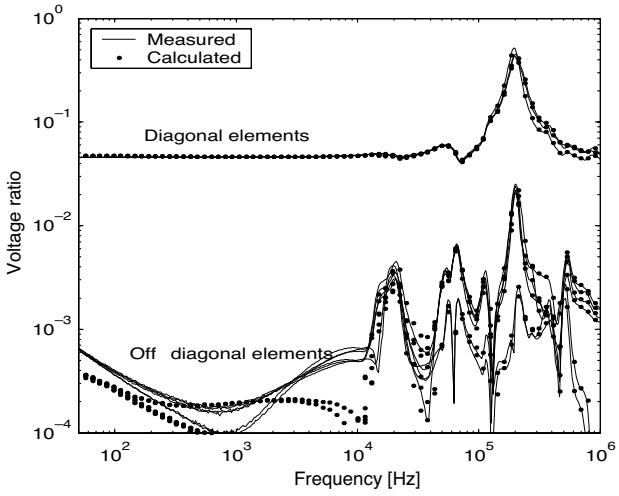

Fig. 7. Measured and calculated elements of V_{LH}.

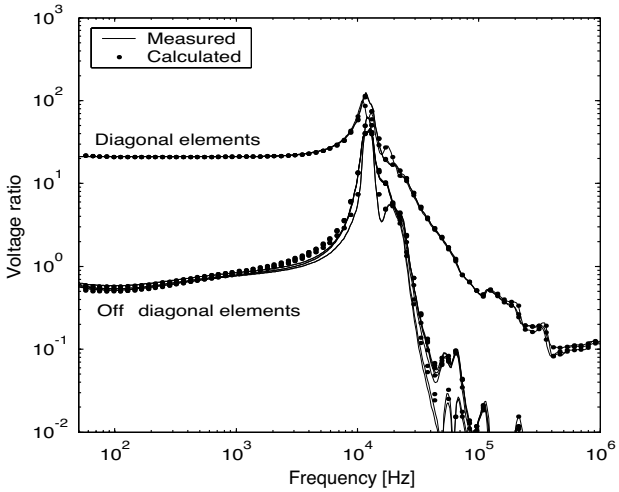

Fig. 8. Measured and calculated elements of V_{HL}.

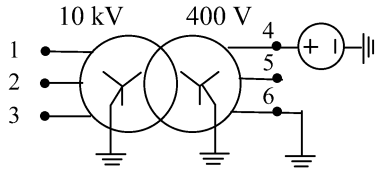

Fig. 9. Open terminals at both windings.

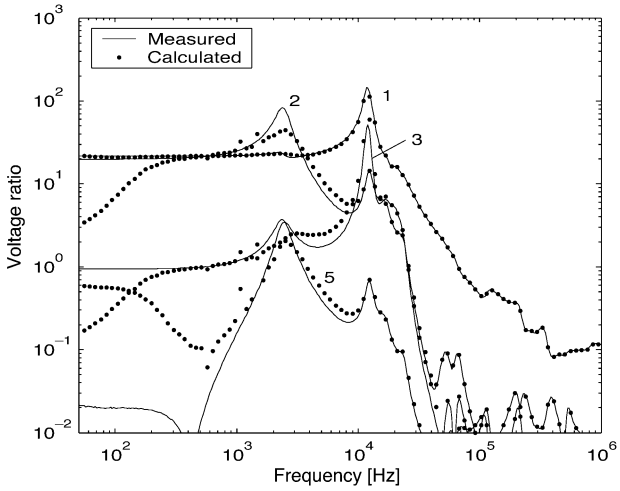

Fig. 10. Measured and calculated voltages at terminals 1, 2, 3, 5 in Fig. 9.

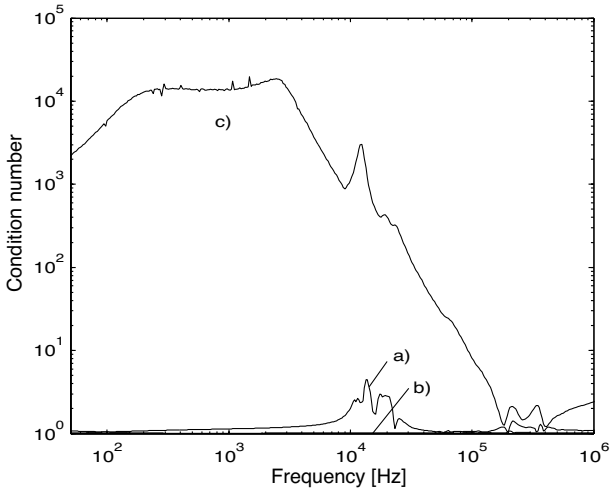

Fig. 11. Condition number for matrix subject to inversion. (a) Y_{HH}, (b) Y_{LL}, (c) Y_A for situation in Fig. 9.

C. Analysis

The above results regarding accuracy can be understood by considering the condition number of the submatrix which is subject to inversion, as explained in Section IV. Fig. 11 compares the condition number κ for the terminal situation in Figs. 7, 8, and 10. It can be seen that for the situation in Fig. 10 (trace "c"), κ is large, particularly at low frequencies which is where the deviation between the measured and calculated voltage ratio is the highest. The small κ for the situation in Figs. 7 and 8 (traces "b," "a") explains the good agreement between the measured and calculated voltage ratio.

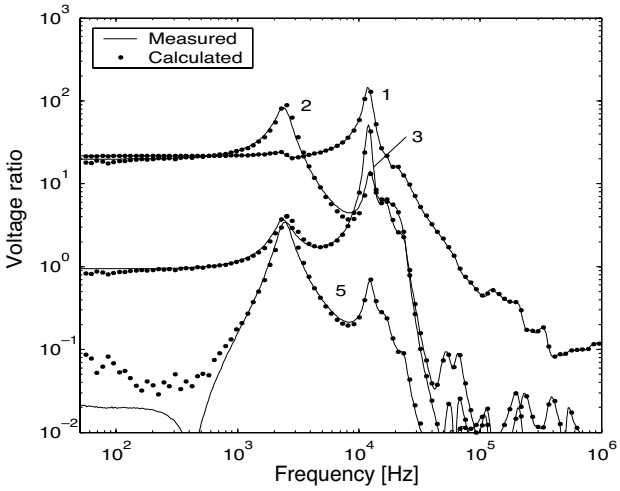

Fig. 12. Calculated versus measured voltage ratio after introducing measured voltage ratios V_{LH} and V_{HL} in the admittance matrix Y.

TABLE I
TRANSFORMER DATA AT 50 HZ, REF. HIGH VOLTAGE SIDE

	Measured[1]	Measured[2]	Nominal
Short circuit imp. [Ω]	124.7	122.6	127
Open circuit imp. [Ω]	566	11771	–
Voltage ratio	20.1	21.7	21.7

VI. INCREASING THE ACCURACY OF THE DATA SET

The accuracy of the transformer model in open circuit conditions can be increased by introducing the measured voltage ratio into the model. The most relevant situation is that all terminals are open on either the high voltage or the low voltage winding. This situation can be modeled by making the following substitutions:

$$Y'_{LL} = Y_{LL} \tag{7}$$

$$Y'_{LH} = -Y'_{LL}V_{LH} \tag{8}$$

$$Y'_{HL} = Y'_{LH} \tag{9}$$

$$Y'_{HH} = -Y'_{HL}V_{HL}^{-1}. \tag{10}$$

The modified Y gets a voltage ratio from high to low and from low to high, which equals the measured voltage ratios.

It was also found that this substitution greatly improves the accuracy for the terminal condition in Fig. 9 (see Fig. 12). Comparison with Fig. 10 shows that the error has been strongly reduced.

The accuracy at 50 Hz can be assessed by comparison with nominal data. Table I shows results for the positive sequence system as calculated from Y, before and after making changes (7)–(10). Both measurements give a short circuit impedance which agrees well with the nominal one. However, the open circuit impedance using the original Y is much too low. Normally, the magnetizing current is much smaller than the nominal load current. 566 Ω gives a current (10.2 A) which is higher than the nominal current (1.73 A). With the modified Y, the current is reduced to 0.49 A. When measuring the admittance with open terminals at the LV-side, a value of 22 002 Ω was achieved, which gives a current of 0.27 A.

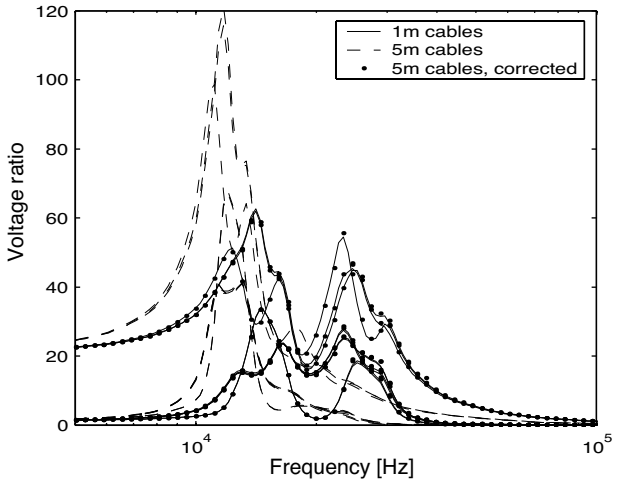

Fig. 13. Calculated voltage ratio. Mitigating the effect of the measuring cables.

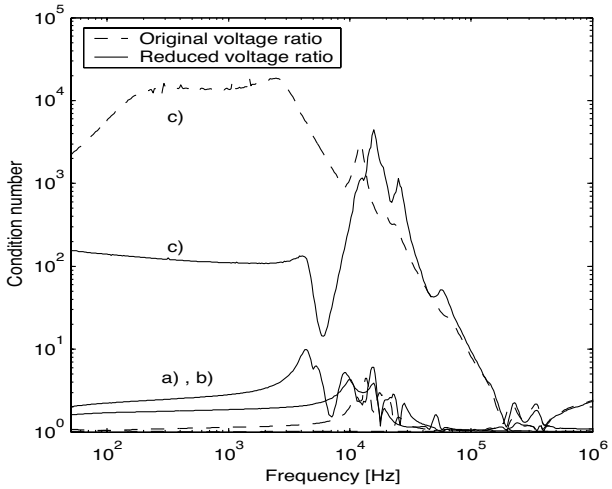

Fig. 14. Effect of reduced voltage ratio on condition number for matrix subject to inversion. (a) Y_{HH}, (b) Y_{LL}, and (c) Y_A for situation in Fig. 9.

The nominal voltage ratio was 10.000/400 = 25 for the original transformer with a Z-connected LV-winding. A Z-connected winding is designed so that the induced voltage in a phase equals the vector sum of two terms of the same length that are displaced by 60° with respect to each other. Therefore, the induced voltage on the secondary becomes increased by a factor of 1/cos30° when reconnecting the secondary into a Y-winding, giving a voltage ratio of 21.7. It is seen in Table I that this modified nominal voltage ratio agrees with the measured voltage ratio.

VII. Correcting for Measurement Cables

The results shown in Figs. 6–12 were obtained with measurement cables of length 5 m. Fig. 13 compares the calculated voltage ratio V_{HL} by (4) when Y was measured using cables of length 1 and 5 m, respectively. Also is shown the response when correcting Y using (6) when C is taken as the difference between the cable capacitances. It is seen that the additional cable length has a strong influence on the transferred voltage and that (6) gives a nearly perfect correction of the cable effect.

VIII. Significance of Nominal Voltage Ratio

For the considered transformer, it was found that the condition number κ becomes high whenever terminals at both the low voltage side and the high voltage side are open. This result can be explained by considering that the magnetizing current is very low compared to the short circuit currents. For a simple T-equivalent representation of a Y-connected transformer without magnetizing branch, one gets an admittance matrix of the form

$$Y = \begin{bmatrix} Y_1 & -aY_1 \\ -aY_1 & a^2Y_1 \end{bmatrix} \tag{11}$$

where a is the nominal voltage ratio and each submatrix Y_1 is nearly diagonal.

In the situation that both neutrals are grounded, Y has three zero eigenvalues and so it cannot be inverted. However, each block in (11) is invertible and so the voltage ratio can be calculated from Y when either of the windings are open-circuited as Y_A in (3) is invertible. But if one or more terminals are open at *both* sides of the transformer, the resulting Y_A gets one or more zero eigenvalues (infinite condition number) and its inverse cannot be computed.

If one includes the magnetizing branch in the T-equivalent, the matrices Y_1 in (11) become slightly different, giving

$$Y = \begin{bmatrix} Y_{11} & -aY_{12} \\ -aY_{21} & a^2Y_{22} \end{bmatrix} \tag{12}$$

where each submatrix is nearly diagonal. It can readily be shown that the presence of a large a leads to an increase of the condition number of Y. Whenever both windings have one or more terminals open, the resulting Y_A in (3) becomes composed of elements from all blocks in (12) and gets a high condition number. Thus, transformers with a high nominal voltage ratio can be expected to be more difficult to model when *both* windings have one or more open terminals.

In order to verify this reasoning, the transformer was modified by disconnecting about 80% of the length of the high-voltage winding, thereby reducing the voltage ratio from 25 to about 5. Fig. 14 shows how the reduction of the voltage ratio affects the condition number of the submatrix subject to inversion, for the examples in Fig. 11. It is seen that the condition number which corresponds to a situation with open terminals at both windings (trace "c"), is reduced by about a factor 100 between 50 Hz and 5 kHz.

IX. Modeling

A. Rational Approximation

The measured Y was modified by introducing the measured voltage ratio by steps (7)–(10), and symmetry was enforced for the resulting Y. The technique of fitting Y with a common set of poles [11] using vector fitting [12] was found to be unsatisfactory for the smallest elements, due to the large variation in the size of the matrix elements, see Fig. 6. The accuracy was substantially increased by partitioning Y into its submatrices Y_{HH}, Y_{HL}, Y_{LH}, Y_{LL}, which were independently subjected to fitting using a common set of poles. The realization A—E from the

four approximations were finally combined into a single combination as shown in (13)–(17), where subscripts 1 and 2 denote H and L, respectively. Note that A is diagonal and that each submatrix of B is sparse

$$A = \mathrm{diag}\left([\mathrm{A}_{11} \quad \mathrm{A}_{21} \quad \mathrm{A}_{12} \quad \mathrm{A}_{22}]\right) \tag{13}$$

$$B = \begin{bmatrix} B_{11} & 0 \\ B_{21} & 0 \\ 0 & B_{12} \\ 0 & B_{22} \end{bmatrix} \tag{14}$$

$$C = \begin{bmatrix} C_{11} & 0 & C_{12} & 0 \\ 0 & C_{21} & 0 & C_{22} \end{bmatrix} \tag{15}$$

$$D = \begin{bmatrix} D_{11} & D_{12} \\ D_{21} & D_{22} \end{bmatrix} \tag{16}$$

$$E = \begin{bmatrix} E_{11} & E_{12} \\ E_{21} & E_{22} \end{bmatrix}. \tag{17}$$

The procedure for fitting the blocks of Y with a common set of poles follows the one outlined in [11]. This procedure utilizes a sparse version of VF which permits individual, frequency dependent weighting of the elements of the considered block of Y. The particular weighting adopted was

$$\mathrm{weight}_{i,j}(s) = \frac{1}{|Y_{i,j}(s)|}. \tag{18}$$

This gives increased weight where elements are small, thus tending to provide a fitting with a high relative accuracy rather than a high absolute accuracy.

The number of iterations needed by VF was strongly reduced by calculating a suitable set of starting poles. This was achieved by first calculating the modes of the considered block of Y, stacking the modes into a single vector and subjecting this vector to fitting by VF. The resulting poles were then taken as starting poles for VF when fitting the block.

Fig. 15 shows the fitted elements of Y using 80 poles per submatrix. The increased error in the voltage transfer due to the rational approximation was negligible for the example in Fig. 7 and 8 (open HV side, open LV side). However, for the example in Fig. 9, the error increased noticeably around 3 kHz, as shown in Fig. 16. This is probably a result of the high condition number causing a magnification of the fitting error.

B. Passivity Enforcement

Passivity was enforced for the rational approximation in order to ensure a stable time domain simulation. Passivity entails that all eigenvalues of the real part of Y are positive for all s, that is

$$\mathrm{eig}\left(\mathrm{Re}\left\{Y_{\mathrm{fit}}(s)\right\}\right) > 0. \tag{19}$$

Passivity was enforced for Y_{fit} by the QP-approach described in [13]. Frequency dependent weighting for the individual elements of Y was introduced in the least-squares problem in QP using the same weighting as in (18). The effect on the voltage transfer in Figs. 7, 8, and 12 was negligible as only a very small correction was needed.

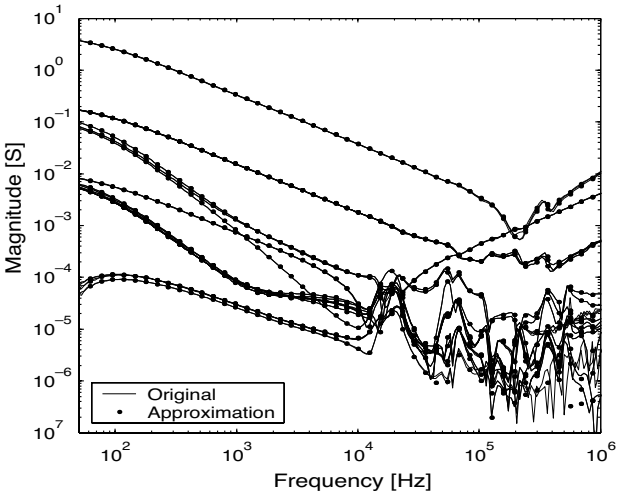

Fig. 15. Rational function approximation of $Y(s)$.

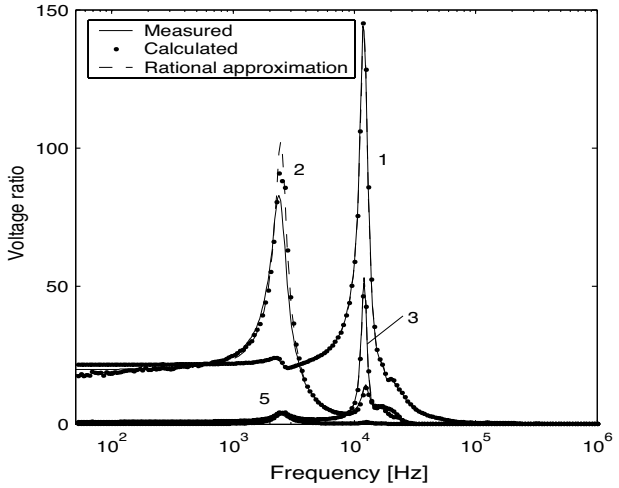

Fig. 16. Voltage transfer of rational approximation versus measured response.

C. Time Domain Implementation

The resulting approximation in the form of matrices A—E can be included in EMTP-type programs as a conductance matrix in parallel with a vector of past history current sources (see [11] for an explanation). A user-defined routine was written for this purpose and included in MatTran [14] which is an EMTP-type program implemented in Matlab.

X. Time Domain Results

A. Energization From Impulse Generator

The following figures compare voltage responses measured directly on the transformer terminals with simulated responses by the model which was obtained using 5-m-long measurement cables. The applied voltage was taken as a known quantity in the simulations.

Fig. 17 shows an example where a near step voltage is applied to terminal 1 on the HV-side with the LV terminals open. The comparison in Fig. 18 between measured and simulated voltages on the LV-side shows a good agreement, although a small deviation in the fundamental frequency can be observed for the voltage on terminal 4.

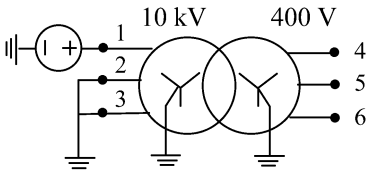

Fig. 17. Excitation on high-voltage side.

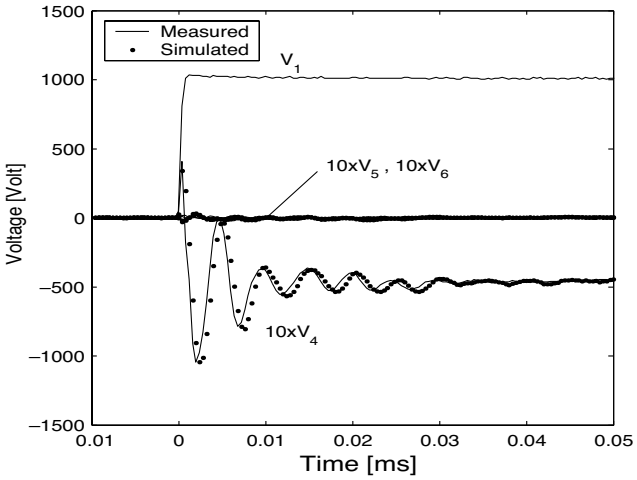

Fig. 18. Voltage responses on low-voltage side.

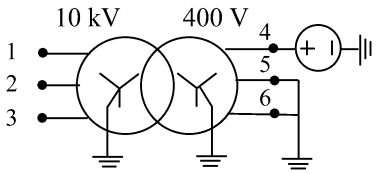

Fig. 19. Excitation on low-voltage side.

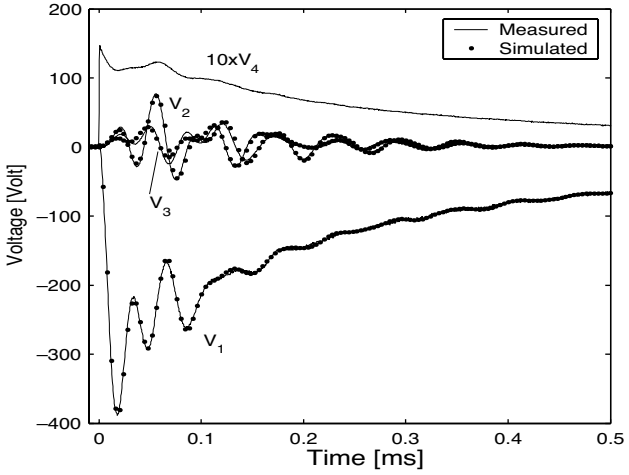

Fig. 20. Voltage responses on high-voltage side.

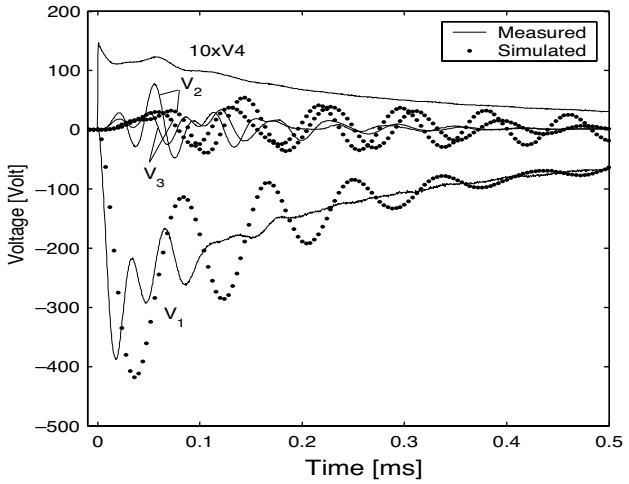

Fig. 21. Voltage responses when the cable capacitances are not accounted for.

Fig. 19 shows an example where a near step voltage is applied to terminal 4 on the LV-side with the HV terminals open. Fig. 20 shows a very good agreement between measured and simulated voltages on the HV side.

Fig. 21 shows the same comparison as in Fig. 20 when the capacitive effect of the measuring cables has *not* been removed from the model by (6). It is seen that very large errors result in the simulated responses. Clearly, the effect of the cable capacitances cannot be neglected.

Fig. 22 considers the situation with open terminals at both sides of the transformer, which was analyzed in the frequency domain in Section V. Fig. 23 shows the resulting voltage on the open terminals. It is seen that the voltage on terminal 2 contains a low-frequency component with too weak attenuation. This corresponds to the deviation at 3 kHz observed in Fig. 16.

B. Transformer With Reduced Voltage Ratio

Fig. 24 shows the same example as in Fig. 23, but after modifying the transformer by reduction of its voltage ratio as was described in Section VIII. It is seen that the accuracy of the low-frequency component in V_2 is higher than in Fig. 23. This improvement can be a result of the reduction of the condition number seen in Fig. 14(c) at low frequencies.

C. Energization From Power Frequency Source

Fig. 25 shows a situation where the transformer (original voltage ratio) is energized at the high-voltage terminals from a three-phase power source. One of the terminals is open on the high-voltage side to represent a broken conductor. The two starpoints were grounded locally at the transformer tank, with the tank potential floating with respect to ground. The voltage measurements were made with the tank as reference ground.

Fig. 26 shows the measured and simulated responses for this situation. The measured voltages at terminals 1 and 2 were taken as known quantities and used as ideal voltage sources in the simulation. It is seen that the simulated waveforms on terminals 4 and 6 are simulated with a high degree of accuracy, including both the 50-Hz component, the initial transient, and the superimposed harmonics. It is noted that a reduced voltage was used in the energization so that no saturation effects would take place.

XI. Discussion

The effect of the capacitance of the measurement cables was taken into account by subtracting the measured capacitance from the measured Y. This procedure can be expected to be accurate as long as the cable capacitance is not much larger

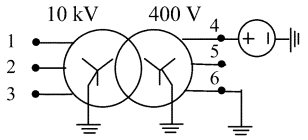

Fig. 22. Open terminals at both windings.

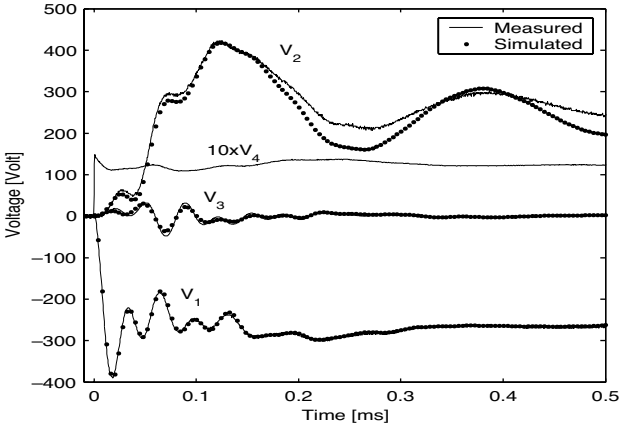

Fig. 23. Voltage response on high-voltage side.

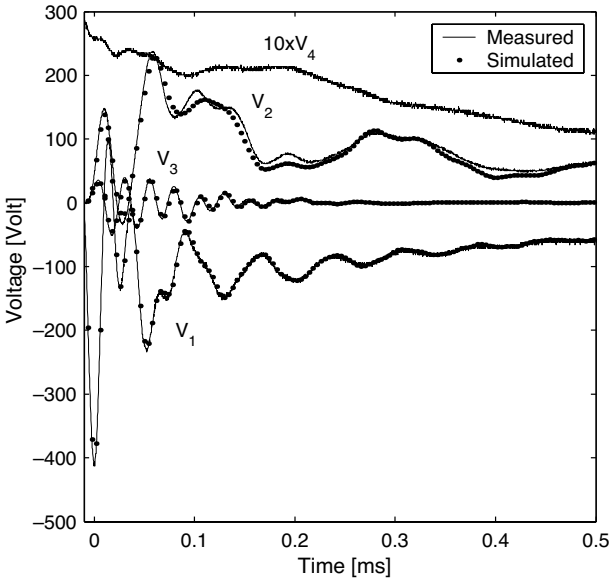

Fig. 24. Voltage response on high-voltage side.

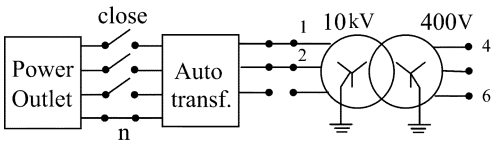

Fig. 25. Energization from 50-Hz power source.

than the transformer capacitance seen at the terminals. The cable capacitance was about 100 pF/m so that 5-m-long cables gives a shunt capacitance of 0.5 nF. The resulting transformer model, including the cable, was found to have a capacitance on the high voltage side of 0.66 nF (average value of three diagonal elements). Subtraction of 0.5 nF gives a remainder

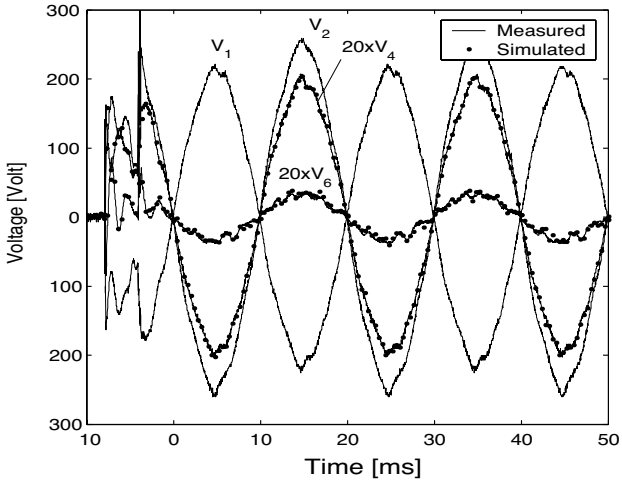

Fig. 26. Measured and simulated voltage waveforms.

of 0.16 nF. It is possible that errors in this subtraction are responsible for some of the deviations between measured and simulated waveforms in Section X. In particular, it was found that when calculating a model using 1-m-long cables, the error in V_4 in Fig. 18 was strongly reduced. (The capacitance on the low-voltage side was 1.34 nF, resulting in 0.84 nF without the cable.)

The sensitivity of the model to errors in measurements and the rational approximation was found to be very high when one or more terminals were open-circuited on both sides of the transformer. Thus, a transformer model may, in general, produce accurate results in one situation and inaccurate results in a different situation. Analysis of the measurements using matrix condition number and redundant measurements are useful tools for detecting such conditions. In this investigation, it was found that the sensitivity due to measurement errors could be strongly reduced by introduction of measured transferred voltages. It was also found that the sensitivity decreased when reducing the voltage ratio of the transformer.

For transformers with ungrounded windings, a high sensitivity to measurement errors can arise even when only one of the windings has open-circuited terminals. A practical remedy for this situation is described in [15].

The comparison between measured and simulated waveforms in Section X has demonstrated that the model can reproduce high-frequency transient waveforms with a high degree of accuracy, including the 50-Hz component. One has to be aware, however, that saturation is not taken into account in the model so that erroneous results may result at low frequencies, particularly at 50 Hz.

XII. Conclusions

A measurement setup has been designed for wide band frequency domain measurement of admittances and transferred voltages on transformers. The setup is based on a network analyzer, shielded cables, a connection board, a current sensor, and voltage sensors. The capacitive effect of the cables is removed from the measured admittance matrix by subtraction of their associated shunt admittances. This setup has the advantage of

accurate measurements, fast reconnections, and reproducible results.

Application to a distribution transformer has demonstrated the accuracy of the procedure by comparison with redundant measurements. The resulting model was, however, found to be sensitive to errors when terminals were open-circuited at both windings. It was found that the accuracy could be greatly improved for this situation by including measured transferred voltages in the model. The sensitivity became reduced at low frequencies when reducing the voltage ratio of the transformer.

A linear model suitable for EMTP-type programs was obtained by subjecting Y to rational approximation and subsequent passivity enforcement. Comparison between measured and simulated time domain voltages have demonstrated a high accuracy of the model both at high frequencies and at 50 Hz.

ACKNOWLEDGMENT

The author expresses his thanks to Prof. K. Feser and the staff at the Institut für Energieübertragung und Hochspannungstechnik, University of Stuttgart, Stuttgart, Germany, for providing laboratory facilities and support of this project. Useful discussions with Dr. T. Henriksen at SINTEF Energy Research is appreciated regarding the usage of transferred voltages in transformer modeling. This work was carried out at the University of Stuttgart.

REFERENCES

[1] P. I. Fergestad and T. Henriksen, "Transient oscillations in multiwinding transformers," *IEEE Trans. Power App. Syst.*, vol. PAS-93, pp. 500–509, Mar./Apr. 1974.

[2] R. C. Degeneff, "A general method for determining resonances in transformer windings," *IEEE Trans. Power App. Syst.*, vol. PAS-96, pp. 423–430, Mar./Apr. 1977.

[3] P. T. M. Vaessen, "Transformer model for high frequencies," *IEEE Trans. Power Delivery*, vol. 3, pp. 1761–1768, Oct. 1988.

[4] G. B. Gharehpetian, H. Mohseni, and K. Möller, "Hybrid modeling of imhomogenous transformer windings for very fast transient overvoltage studies," *IEEE Trans. Power Delivery*, vol. 13, pp. 157–163, Jan. 1998.

[5] Q. Su, R. E. James, and D. Sutanto, "A z-transform model of transformers for the study of electromagnetic transients in power systems," *IEEE Trans Power Syst.*, vol. 5, pp. 27–33, Feb. 1990.

[6] A. Morched, L. Marti, and J. Ottevangers, "A high frequency transformer model for the EMTP," *IEEE Trans. Power Delivery*, vol. 8, pp. 1615–1626, July 1993.

[7] T. Hasman, "Reflection and transmission of traveling waves on power transformers," *IEEE Trans. Power Delivery*, vol. 12, pp. 1684–1689, Oct. 1997.

[8] B. Gustavsen and A. Semlyen, "Application of vector fitting to the state equation representation of transformers for simulation of electromagnetic transients," *IEEE Trans. Power Delivery*, vol. 13, pp. 834–842, July 1998.

[9] Course EE263: Introduction to Linear Dynamical Systems, Lecture notes from Prof. S.P. Boyd, Stanford University, CA.

[10] L. N. Trefethen and D. Bau, *Numerical Linear Algebra*. Philadelphia, PA: SIAM, ISBN 0–89871–361–7, 1997, p. 95.

[11] B. Gustavsen, "Computer code for rational approximation of frequency-dependent admittance matrices," *IEEE Trans. Power Delivery*, vol. 17, pp. 1093–1098, Oct. 2002.

[12] B. Gustavsen and A. Semlyen, "Rational approximation of frequency domain responses by vector fitting," *IEEE Trans. Power Delivery*, vol. 14, pp. 1052–1061, July 1999.

[13] ——, "Enforcing passivity for admittance matrices approximated by rational functions," *IEEE Trans. Power Syst.*, vol. 16, pp. 97–104, Feb. 2001.

[14] J. Mahseredjian and F. Alvarado, "Creating an electromagnetic transients program in Matlab: MatEMTP," *IEEE Trans. Power Delivery*, vol. 12, pp. 380–388, Jan. 1997.

[15] B. Gustavsen, "Frequency dependent modeling of power transformers with ungrounded windings," IEEE Trans. Power Delivery, to be published.

Bjørn Gustavsen (M'94–SM'03) was born in Harstad, Norway, in 1965. He received the M.Sc. and Dr.-Ing. degrees from the Norwegian Institute of Technology, Trondheim, in 1989 and 1993, respectively.

Currently, he is with SINTEF Energy Research, Trondheim. His interests include simulation of electromagnetic transients and modeling of frequency-dependent effects. He spent 1996 as a Visiting Researcher at the University of Toronto, Toronto, ON, Canada, and the summer of 1998 at the Manitoba HVDC Research Center, Winnipeg, MB, Canada.